ROYAL SOCIETY
OF CHEMISTRY

COMMUNICATION

Check for updates

Metal cation substitution can tune CO_2, H_2O and CH_4 switching pressure in transiently porous coordination networks†

Varvara I. Nikolayenko, ‡[a] Dominic C. Castell, ‡[a] Debobroto Sensharma, [a] Mohana Shivanna,[b] Leigh Loots, [c] Ken-ichi Otake, [b] Susumu Kitagawa,[b] Leonard J. Barbour [c] and Michael J. Zaworotko *[a]

Compared to rigid physisorbents, switching coordination networks that reversibly transform between closed (non-porous) and open (porous) phases offer promise for gas/vapour storage and separation owing to their improved working capacity and desirable thermal management properties. We recently introduced a coordination network, **X-dmp-1-Co**, which exhibits switching enabled by transient porosity. The resulting "open" phases are generated at threshold pressures even though they are conventionally non-porous. Herein, we report that **X-dmp-1-Co** is the parent member of a family of transiently porous coordination networks **[X-dmp-1-M]** (M = Co, Zn and Cd) and that each exhibits transient porosity but switching events occur at different threshold pressures for CO_2 (0.8, 2.1 and 15 mbar, for Co, Zn and Cd, respectively, at 195 K), H_2O (10, 70 and 75% RH, for Co, Zn and Cd, respectively, at 300 K) and CH_4 (<2, 10 and 25 bar, for Co, Zn and Cd, respectively, at 298 K). Insight into the phase changes is provided through *in situ* SCXRD and *in situ* PXRD. We attribute the tuning of gate-opening pressure to differences and changes in the metal coordination spheres and how they impact dpt ligand rotation. **X-dmp-1-Zn** and **X-dmp-1-Cd** join a small number of coordination networks (<10) that exhibit reversible switching for CH_4 between 5 and 35 bar, a key requirement for adsorbed natural gas storage.

Introduction

Owing to the energy-intensive requirements associated with current gas storage and delivery technologies, such as compression and liquefaction, more energy efficient

approaches are being investigated.[1] In general, physisorption by porous solids[2–5] offers potential for significantly improving the energy footprint associated with industrial gas storage. This is especially the case for the *ca.* 118 000 porous coordination networks (PCNs)[6–8] whose crystal structures have been deposited in the Cambridge Structural Database (CSD),[9,10] most of which are classified as metal–organic frameworks (MOFs).[11–15] PCNs, some of which are highly amenable to design,[14] are typically rigid according to their Type-I gas sorption isotherm profiles. Unfortunately, rigid physisorbents tend to suffer from reduced working capacities in gas storage applications since Type-I isotherms necessarily mean that working capacity will be less than total uptake, regardless of the operationally relevant pressure range (Fig. 1, blue).[16]

Switching flexible metal–organic materials (FMOMs)[16,17] are a small subset of PCNs that exhibit guest-induced phase transformations from a closed (non-porous) to an open (porous) phase(s) over a narrow pressure range. Such sorbents exhibit stepped or Type F-IV isotherms, which can enable working capacities to equal total uptake when the step occurs between loading and delivery pressures (Fig. 1, green). FMOMs could offer a practical solution to gas storage/delivery applications and are of particular interest with respect to adsorbed natural

aDepartment of Chemical Sciences, Bernal Institute, University of Limerick, Limerick V94T9PX, Republic of Ireland. E-mail: xtal@ul.ie

bInstitute for Integrated Cell-Material Sciences (iCeMS), Institute for Advanced Study, Kyoto University (KUIAS), Yoshida Ushinomiyacho, Sakyoku, Kyoto 606-8501, Japan

cDepartment of Chemistry and Polymer Science, University of Stellenbosch, Matieland 7600, South Africa
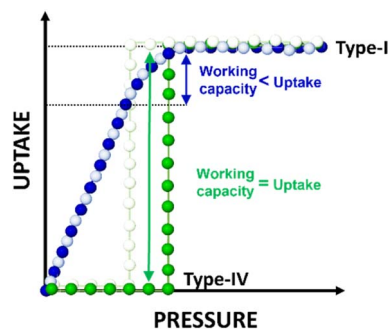
‡ These authors contributed equally.

Fig. 1 Comparison of Type-I (blue) and Type-IV (green) physisorbent isotherm types. Desorption profiles are shown as open spheres. Type-IV isotherms offer higher working capacities than Type-I isotherms.

gas (ANG),[18] for which they already offer volumetric working capacities close to that of compressed natural gas (CNG).[19–21] Of the approximately 100 switching FMOMs reported to date,[17] only a handful have been subjected to systematic crystal engineering studies (*e.g.* ligand functionalisation,[19–21] complete ligand substitution[22,23] or metal cation substitution[24–31]). These examples typically transform from non-porous to porous phase(s) with large, sometimes extreme, structural changes. Tuning of the Type F-IV isotherm is not always feasible since change in composition, even of a single atom, can result in a different sorption mechanism and isotherm type.[32]

Rarer still is a class of sorbents where sorption occurs through the counterintuitive diffusion mechanism of *transient porosity*, wherein guest transport occurs between isolated cavities despite the absence of interconnecting channels. This phenomenon was first illustrated in the bowl-shaped molecular organic solid *p-tert*-butylcalix[4]arene.[33] Thereafter, several other examples of non-porous molecular solids demonstrating this behaviour were reported,[34–41] none of which exhibited stepped gas sorption isotherms. Separate studies conducted by the Kitagawa and Barbour groups reported on guest transport in FMOMS with either pores connected by discrete apertures, or isolated voids.[42–45] Although the latter example shows a switching isotherm, it has an as-synthesised phase with a channel-type structure.

We recently reported the first example of a PCN with transient porosity, [Co(dpt)(1,3-bib)·2DMF] (**X-dmp-1-Co**, Fig. 2a, pink), where dpt = 5-diphenylbenzene-1,4-dicarboxylic acid and 1,3-bib = 1,3-bis(imidazol-1-yl)benzene.[46] This clathrate underwent a series of guest-induced phase transformations while remaining conventionally non-porous. Computational experiments indicated that the likely mechanism of guest transport was enabled by subtle motion of both the dpt and 1,3-bib ligands, arising from metal node isomerism involving coordination bond breakage. Although rare, this phenomenon was already known to occur in switching FMOMs.[47,48] As a result, the dynamic and cooperative motion of host framework components creates transient windows for guest molecules to diffuse between otherwise isolated cavities.[44,46]

In this contribution, we address the effect of metal substitution on transient porosity in FMOMS through study of the Zn and Cd analogues of **X-dmp-1-M** (Fig. 2). Insight into the dynamic behaviour of **X-dmp-1-M** is provided by single-crystal X-ray diffraction (SCXRD), gas and/or vapour sorption and *in situ* powder X-ray diffraction (PXRD), thereby allowing us to draw direct comparisons between the CO_2-, CH_4- and H_2O-induced phase transformations present in these transiently porous systems, and in turn, their sorption isotherm profiles.

Experimental

Materials

1,3-bib and dpt where synthesised according to the previously reported procedures.[46] All purchased chemicals were used as received without further purification.

Synthesis of X-dmp-1-M-α (M = Co, Zn, Cd)

Crystals suitable for SCXRD analysis of the as-synthesised forms **X-dmp-1-M-α** (M = Co, Zn, Cd) were prepared solvothermally by heating a sealed 28 mL glass vial of the appropriate metal nitrate salt (0.3 mmol), dpt (0.3 mmol), 1,3-bib (0.3 mmol) and dimethylformamide (DMF, 10 mL) in an oven at 120 °C. Purple, colourless and pale-yellow crystals were obtained after 24 hours, respectively.

Formation of X-dmp-1-M-β (M = Co, Zn, Cd)

Single-crystals of the guest-free forms **X-dmp-1-M-β** were obtained by soaking the crystals of **X-dmp-1-M-α** in methanol for two days and then evacuating under dynamic vacuum at 70 °C for 10 hours using a Micromeritics Smart VacPrep instrument.

Results and discussion

The crystal structures of the as-synthesised and guest-free forms of **X-dmp-1-Co** were previously determined using SCXRD[46] and are used for comparison with the structures of **X-dmp-1-Zn** and **X-dmp-1-Cd** determined herein. All three as-synthesised forms of **X-dmp-1-M** crystallise in the monoclinic space group $P2_1/n$ with one metal cation, one 1,3-bib linker ligand (anti-conformation), two independent half dpt linker ligands and two DMF guest molecules in the asymmetric unit (ASU, Table S1†). The coordination spheres differ between the three as-synthesised phases. In **X-dmp-1-Co-α**, one dpt linker ligand chelates the metal cation whereas the second is mono-coordinated. In **X-dmp-1-Zn-α**, both dpt carboxylate moieties are mono-coordinated whereas in **X-dmp-1-Cd-α** both chelate the metal centre (Fig. 2a). Unlike in **X-dmp-1-Co-α**, where one of the dpt linkers is disordered over two positions, no disorder was observed in the Zn or Cd analogues. All three forms of **X-dmp-1-M-α** are isostructural[49] 3D non-interpenetrated nets with **dmp** topology. Each variant contains solvent-filled discrete voids of 411 Å³, 396 Å³ and 443 Å³, respectively (determined using a Conolly map[50,51] with a 1.5 Å probe radius, Fig. 2a).

Thermogravimetric analysis (TGA, Fig. S11†) revealed that both **X-dmp-1-Zn-α** and **X-dmp-1-Cd-α** exhibit stronger host–guest interactions as well as better thermal stability (*ca.* 378 °C and 360 °C) when compared to **X-dmp-1-Co-α** (*ca.* 325 °C). This variance in stability can be rationalised upon closer examination of the structures of **X-dmp-1-M-β**. Unlike **X-dmp-1-Co-β**, which transforms to a phase in which an aqua ligand is coordinated if exposed to atmospheric conditions (the SCXRD structure was obtained using an environment cell),[46] **X-dmp-1-Zn-β** and **X-dmp-1-Cd-β** were obtained by heating in air (Fig. 2b and Table S1†). A comparison of all three closed phases at 298 K (Fig. 2b, S1 and S2†) reveals that the one of the dpt ligands can act as a turnstile and rotates into the cavity, reducing the guest accessible space to 84 Å³, 39 Å³ and 83 Å³ respectively. In the case of **X-dmp-1-Co-β**, this transformation occurred concomitantly with a change in the coordination mode of the metal centre. For both zinc and cadmium, the coordination around the metal remains unchanged. Furthermore, **X-dmp-1-Cd-β** has
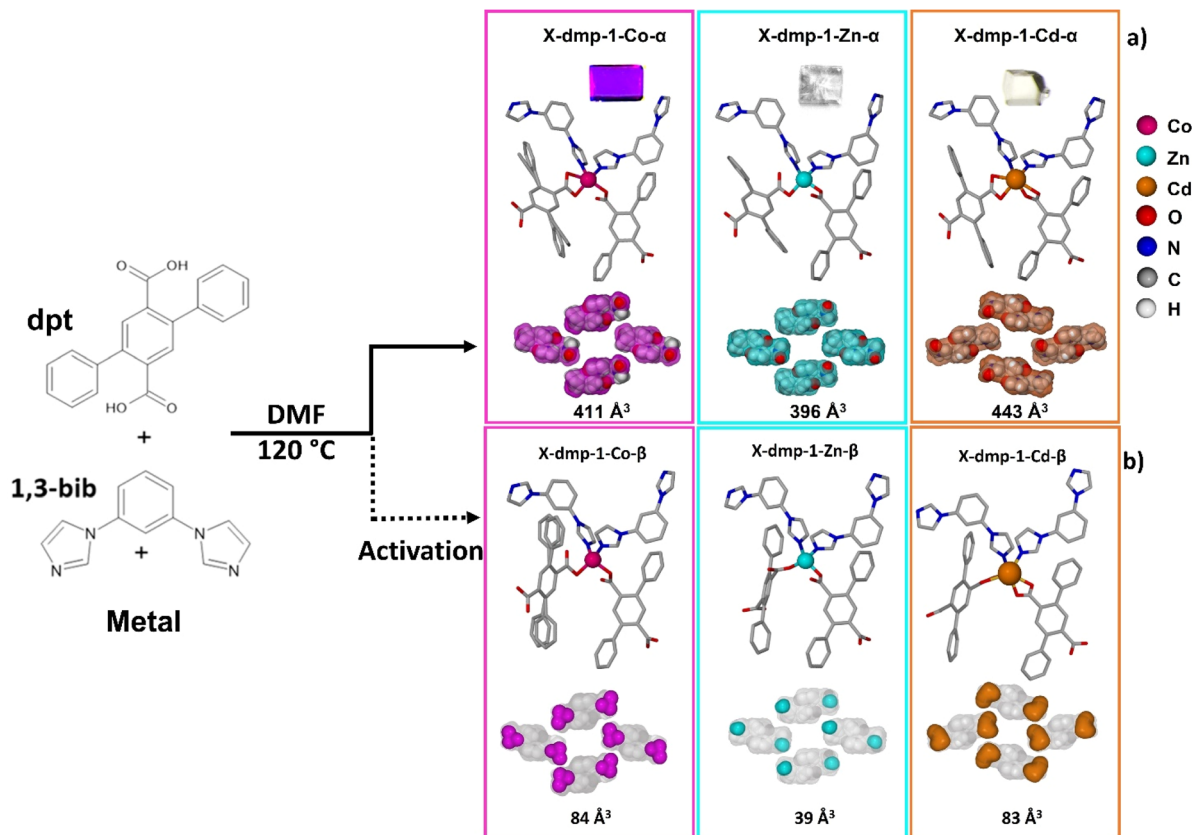
16020 | *J. Mater. Chem. A*, 2023, **11**, 16019–16026

This journal is © The Royal Society of Chemistry 2023

Fig. 2 (a) Solvothermal preparation of **X-dmp-1-M-α** from dpt, 1,3-bib and a transition metal where Co (pink), Zn (cyan) and Cd (orange). The metal node in **X-dmp-1-Co** has one chelating and one mono-coordinated dpt acid while **X-dmp-1-Zn** has two mono-coordinated dpt acids and **X-dmp-1-Cd** has two chelating dpt acids. The guest-accessible discrete cavities occupied by space-filled *N,N*-dimethylformamide (DMF) guest molecules are shown as coloured surfaces (colours coincide with metal colour). Photomicrographs of a single crystal of each form of **X-dmp-1-M** are also shown; (b) activation of **X-dmp-1-M-α** results in a single-crystal to single-crystal phase transformation to **X-dmp-1-M-β** where the coordination mode around the metal centre changes owing to twisting of the dpt ligand. This rotation significantly reduces the guest accessible cavities.

several CH short contacts between the rotating dpt ligand and the surrounding 1,3-bib ligands (Fig. S2†).

To better understand the relationships between **X-dmp-1-M-β** and water vapour, Dynamic Vapour Sorption (DVS) experiments were performed (Fig. S24–S26†). In each case, a powdered sample of **X-dmp-1-M-β** was evacuated before a water vapour sorption isotherm was collected at 27 °C from vacuum to 95% RH (2.85 kPa). Although all three forms exhibited S-shaped isotherms, distinct differences in the inflection RH, uptake and degree of hysteresis were observed. The inflection in **X-dmp-1-Co-β** occurred at 10% RH with a maximum loading of 8 wt% (Fig. S24†). **X-dmp-1-Zn-β** and **X-dmp-1-Cd-β** exhibited inflections at progressively higher RH values (70%, uptake = 18 wt%, and 75% RH, uptake = 15 wt%, respectively) with notable hysteresis. We attribute the lower uptake in the Co variant to aqua complex formation before inflection (reducing its void volume).[46] Since the inflection point is above the ambient RH in the authors' laboratory, the structures of these phases could be crystallographically determined without the use of an environment cell. To date, there are very few examples wherein metal variation has been shown to impart an effect on the water sorption properties of a series of isostructural

PCNs.[52–55] In the cases of **X-dmp-1-Zn-β** and **X-dmp-1-Cd-β**, exposure to water appears to induce a different mechanism of guest loading when compared to **X-dmp-1-Co-β** as evidenced by the almost twofold increase in loading and notable hysteresis. The observed differences in water loading are consistent with an aqua molecule coordinating to the zinc and cadmium cations, followed by pore filling.

Having confirmed bulk phase purity (Fig. S5–S10†), the phase behaviour of **X-dmp-1-M-β** over a broad P/P_0 range was investigated using low temperature 77 K N_2 and 195 K CO_2 gas sorption. BET surface areas corresponding to 516.6 $m^2\ g^{-1}$ and 617.07 $m^2\ g^{-1}$ were determined from the 77 K N_2 sorption isotherms for **X-dmp-1-Co-β** and **X-dmp-1-Zn-β** (Fig. S12, S13, S19 and Table S4†). Owing to the non-porous clathrate nature of **X-dmp-1-M-β**, **X-dmp-1-Co** and **X-dmp-1-Zn** are believed to have very low switching pressures for nitrogen at 77 K, but the exact values could not be reliably quantified. No appreciable N_2 uptake was observed for **X-dmp-1-Cd-β** (Fig. S14†). The phase transformation of **X-dmp-1-M-β** to **X-dmp-1-Co-γ1**, **X-dmp-1-Zn-γ2** and **X-dmp-1-Cd-γ2** (the first gas loaded phase) with CO_2 occurred at low P/P_0 (log plots, Fig. 3) with the threshold pressure trend Co (0.8 mbar) < Zn (2.1 mbar) < Cd (15.0 mbar).
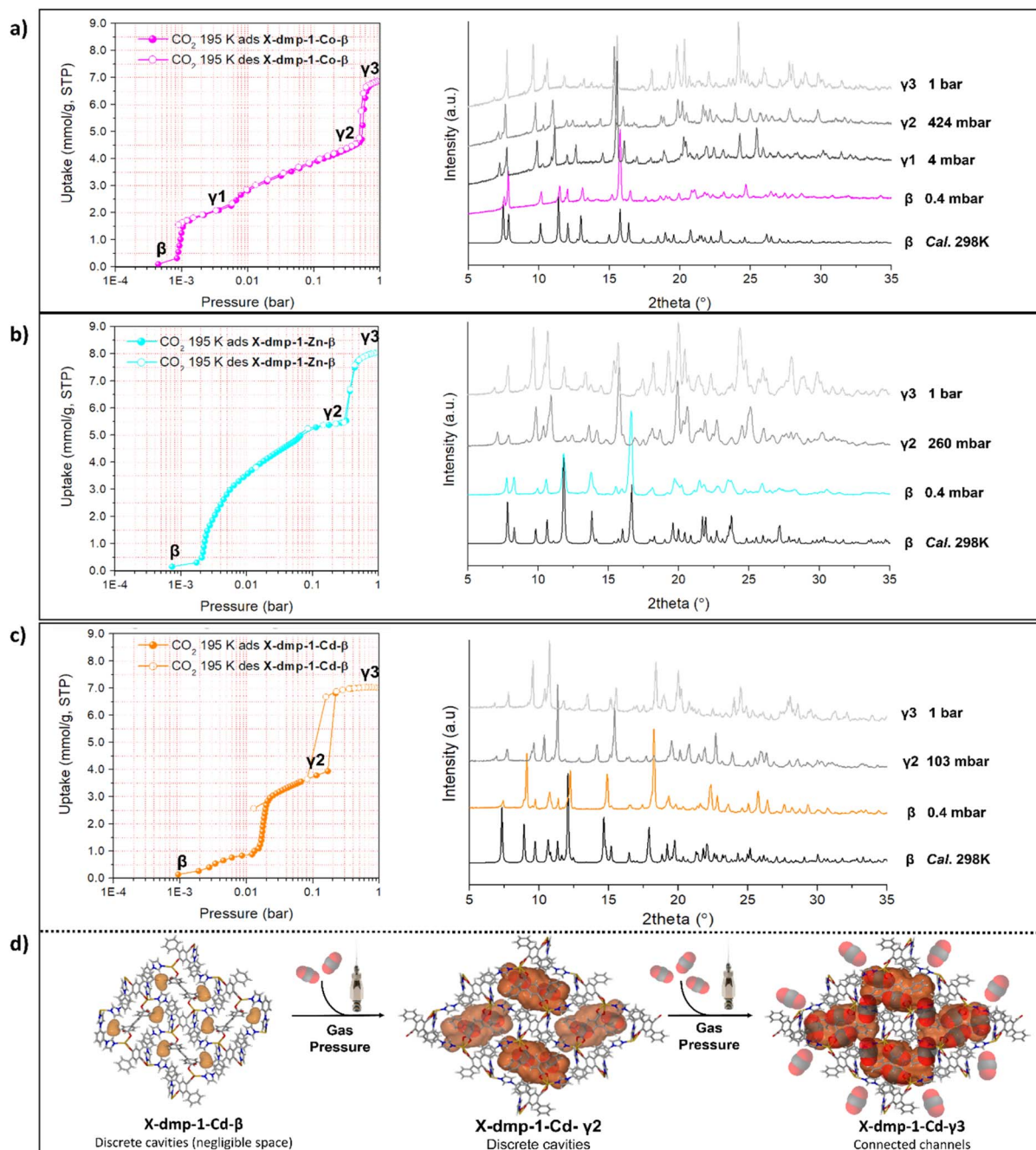
This journal is © The Royal Society of Chemistry 2023

J. Mater. Chem. A, 2023, **11**, 16019–16026 | **16021**

Fig. 3 (Left: (a)−(c)) CO$_2$ 195 K sorption isotherms of **X-dmp-1-M-β** plotted using a logarithmic scale with phases indicated from β-γ3; (right: (a)−(c)) an overlay of corresponding *in situ* variable pressure PXRD patterns ($\lambda = 1.54178$ Å) of **X-dmp-1-M-β** at different CO$_2$ adsorption loadings recorded at 195 K. (d) Packing diagrams illustrating the structural transformations observed in **X-dmp-1-Cd**.

Owing to the discrepancy in loading (Fig. S15†), no γ1 phase was observed in the Zn and Cd analogues (*i.e.* **X-dmp-1-Co-β** exhibits three distinct transformations,[46] while **X-dmp-1-Zn-β** and **X-dmp-1-Cd-β** only exhibit two). The final transformation from γ2 to γ3 occurred with a reverse threshold pressure trend of Co (545 mbar) > Zn (371 mbar) > Cd (220 mbar).

To gain further insight into the nature of the phases associated with these transformations, concurrent *in situ* PXRD data were recorded during the 195 K CO$_2$ sorption experiments of all three **X-**

dmp-1-M-β variants. In each case, the calculated PXRD pattern obtained from the SCXRD experiments was in good agreement with the experimentally obtained 195 K vacuum pattern. Upon exposure to 0.8 (Co), 3.6 (Zn) and 13 (Cd) mbar of CO$_2$, each variant of **X-dmp-1-M-β** underwent a phase transformation to **X-dmp-1-Co-γ1**, **X-dmp-1-Zn-γ2** and **X-dmp-1-Cd-γ2**.

When compared to **X-dmp-1-M-β** the PXRD patterns of these phases (Fig. 3) revealed a shifting of peaks to lower 2θ values, indicative of unit cell expansion. Additionally, new peaks were
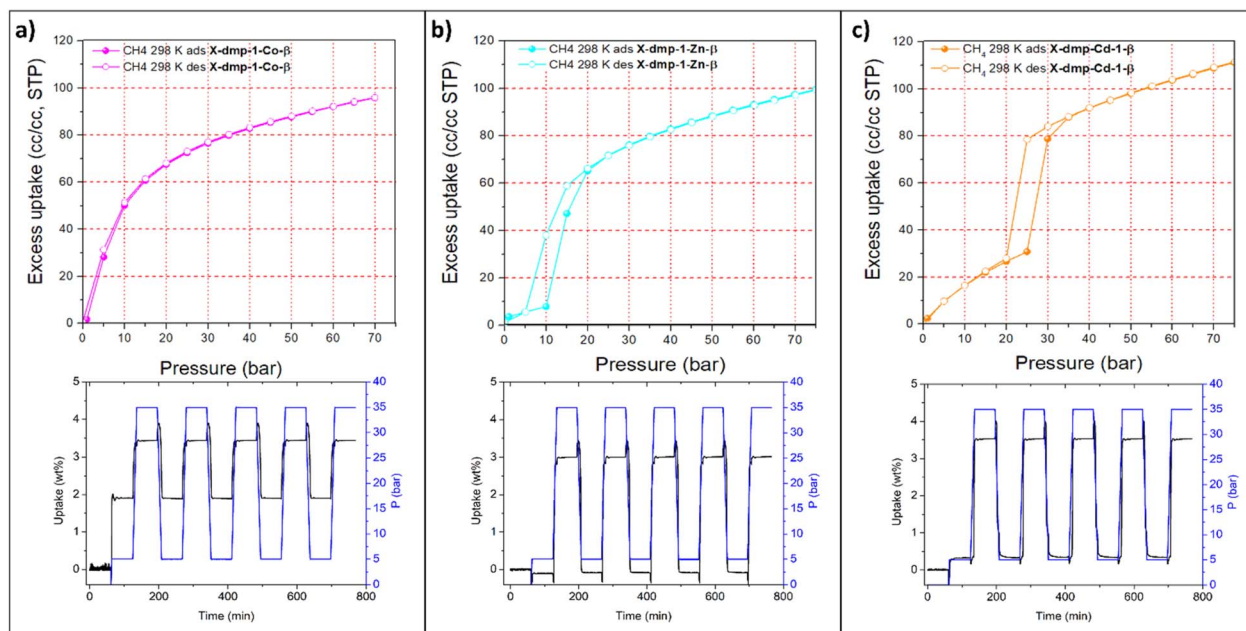
16022 | *J. Mater. Chem. A*, 2023, **11**, 16019–16026

This journal is © The Royal Society of Chemistry 2023

Fig. 4 (Top: (a)–(c)) High pressure CH_4 gas sorption isotherm and dynamic cycling experiments for (a) **X-dmp-1-Co-β**; (b) **X-dmp-1-Zn-β** and (c) **X-dmp-1-Cd-β** collected at 298 K. Adsorption is shown as filled circles while desorption open circles; (bottom: (a)–(c)) CH_4 cycling experiments showing five cycles between 5 and 35 bar at 298 K.

observed (at $2\theta = 12.72°$, $14.52°$, $15.82°$ and $17.0°$ for **X-dmp-1-Zn-γ2** (Fig. S20†) and $2\theta = 7.00°$, $7.72°$, $10.37°$, $12.93°$, $14.22°$ and $15.47°$, for **X-dmp-1-Cd-γ2**, Fig. S21†) while others disappeared (at $2\theta = 13.88°$, $15.67°$ and $23.78°$ for **X-dmp-1-Zn-γ2** and $2\theta = 7.375°$, $8.959°$, $10.72°$, $12.09°$, $14.72°$, and $17.97°$, for **X-dmp-1-Cd-γ2**).

Progressive loading revealed continued peak shifting, culminating in a second transformation from **X-dmp-1-M-γ2** to **X-dmp-1-M-γ3**, for all three metal variants. The PXRD pattens recorded at 1 bar revealed (Fig. 3) lateral shifting with the appearance of peaks at $2\theta = 11.95°$, $13.46°$, and $19.31°$ for **X-dmp-1-Zn-γ3** and $2\theta = 13.51°$, $19.04°$ and $24.51°$ for **X-dmp-1-Cd-γ3**. Overlay comparisons of the three **X-dmp-1-M-γ2** and **X-dmp-1-M-γ3** phases (Fig. S22 and S23†) are in good agreement.

High pressure (40 bar) CO_2 experiments performed on the three **X-dmp-1-M-β** samples (Fig. S16–S18†) revealed that the $\gamma 2$ to $\gamma 3$ transition was only observed for **X-dmp-1-Cd-β** at 273 K. To gain further insight into the structural nature of this final transition, gas loaded *in situ* SCXRD was performed. After backfilling the environment gas cell with CO_2 to the maximum experimentally feasible pressure (56 bar, 298 K), the system was left to equilibrate for 12 h before being sealed (see ESI† for details). SCXRD data were then recorded. Under these conditions, **X-dmp-1-Cd-β** transformed to **X-dmp-1-Cd-γ2** with a 3.75(9) Å increase in the c-axis and a 24% increase in the unit cell volume (Table S1†), resulting in discrete voids of 389 Å^3 or cavities connected by discrete apertures (424 Å^3) depending on the component of disorder used (Fig. S3†). This transformation can once again be attributed to rotation of the dpt ligand.[46] Although the CO_2 guest could not be modelled crystallographically, the residual electron density analysis, as

implemented by the SQUEEZE[56] routine of PLATON,[57] indicated the presence of one CO_2 molecule per ASU. In a final attempt to elevate the P/P_0 value, the environment cell was cooled to 273 K and the data was recollected. Under these sublimation conditions **X-dmp-1-Cd-γ2** converted to **X-dmp-1-Cd-γ3** with minimal change of cell lengths but with a 117 Å^3 increase in the unit cell volume. As computationally postulated by our study of **X-dmp-1-Co-γ3**,[46] the SCXRD structure of **X-dmp-1-Cd-γ3** revealed that the previously discrete channels merge through cooperative motion of both ligands to generate narrow apertures between cavities (Fig. 3d and S4†). As with **X-dmp-1-Cd-γ2**, the CO_2 guest in **X-dmp-1-Cd-γ3** could not be modelled crystallographically a residual electron density consistent with the presence of two CO_2 gas molecules per asymmetric unit.

Since physisorbents can be evaluated for ANG storage applications based on their working capacities between 5 and 35 bar at near ambient temperature,[58–60] we conducted dynamic CH_4 sorption studies on all three **X-dmp-1-M-β** variants at 298 K. Fig. 4 (top) reveals that uptake was significantly lower (100–120 cc/cc) than the current DOE target of >12.5 MJ L^{-1} (360 cc/cc).[58,59] Nevertheless, metal variation in **X-dmp-1-M-β** enabled tuning of the switching pressure. In the case of **X-dmp-1-Co-β**, the conversion from **β** to **γ1** induced by CH_4 occurred at a pressure (<2 bar) that is to our knowledge below that reported for any other FMOM (Table S5†). The threshold pressure for the corresponding phase transformation increased to 10 bar for **X-dmp-1-Zn-β** and to 25 bar for **X-dmp-1-Cd-β**. As a result, **X-dmp-1-Zn** and **X-dmp-1-Cd** would be expected to show significantly higher CH_4 working capacities compared to **X-dmp-1-Co** since the quantity of gas retained at

This journal is © The Royal Society of Chemistry 2023

J. Mater. Chem. A, 2023, **11**, 16019–16026 | **16023**

the unloading pressure is significantly decreased by the phase transformation to β at 5 bar in **X-dmp-1-Zn** and 20 bar in **X-dmp-1-Cd**. This was experimentally confirmed by a series of dynamic cycling experiments (Fig. 4, bottom) between these loading and unloading pressures, in which **X-dmp-1-Zn** and **X-dmp-1-Cd** showed higher gravimetric working capacities for CH_4 (62.31 cc/cc for Zn and 67.17 cc/cc for Cd) than **X-dmp-1-Co** (41.63 cc/cc). After five sorption cycles, no deterioration of working capacity was observed.

Having experimentally observed the effect of metal variation upon the H_2O, CO_2 and CH_4 gas sorption properties in **X-dmp-1-M**, we postulate and attribute the changes in these properties to guest-induced rotations of the dpt ligand that are impacted by the coordination mode around the metal centre.

Conclusions

In summary, we report the effect that metal cation substitution imparts on the switching behaviour of a family of **X-dmp-1-M** CNs induced by H_2O, CO_2 and CH_4 sorption. Metal cation substitution is an established design strategy to impact the properties of physisorbents; however, to our knowledge, we report the first example wherein the nature of the metal cation, coupled with changes in the coordination mode, facilitate tuneable switching in a family of transiently porous networks. Herein, guest transport is facilitated by dynamic and cooperative motion (in the form of rotation of the DPT linker and subtle movement in the 1,3-bib) of the host framework creating momentary windows of opportunity for guest molecules to diffuse between otherwise isolated cavities. While variation of the metal cation (likely a result of different cation size) dictates the inflection point pressure. The CH_4 sorption properties are also of note. Of the approximately 100 FMOMs reported thus far, only 16 (Table S5†) have been shown to exhibit inflected isotherms for CH_4 and none involved systematic study of a family of materials wherein the metal was varied. This low number is ascribed to weak host–guest interactions between CH_4 and most PCNs. Owing to the small kinetic diameter of cobalt (which necessitates that both dpt ligands be mono-coordinated), coupled with the lack of notable interactions in the non-porous clathrate phase **X-dmp-1-Co-β**, it was expected that the energy barrier associated with the first transition in this material would be quite low. Indeed, **X-dmp-1-Co** exhibited the lowest threshold pressure inflection for CH_4 reported to date (<2 bar). The switching pressure for **X-dmp-1-Zn** was 10 bar whereas **X-dmp-1-Cd** loaded CH_4 at 25 bar. We attribute this variance to the size of the metal cation, which in turn affects the coordination around the metal node. For **X-dmp-1-Cd**, both dpt ligands are chelating and, coupled with short CH and OH contacts between the dpt ligand and neighbouring 1,3-bib ligands, the energy barrier required for **X-dmp-1-Cd-β** to switch is expected to be higher than for the other two transition metals. Overall, the metal variation strategy herein serves as a proof-of-concept for CH_4 storage applications in transiently porous CNs as we shifted the switching pressure of CH_4 gas sorption to the operationally relevant range with a 50% increase in working capacity without the need for extreme, structural changes.

Systematic studies such as this can provide guidance for the development of a new generation of industrially practical physisorbents.

Author contributions

M. J. Z. and V. I. N. conceived the original idea. V. I. N. performed the synthesis, characterisation analysis, SCXRD experiments and wrote the draft manuscript. D. C. C. synthesised the ligands (dpt and 1,3-bib), measured the water sorption data and wrote the draft manuscript. D. S. performed gas sorption experiments. M. S., K.-i. O. and S. K. performed *in situ* PXRD experiments. L. L. and L. J. B. conducted *in situ* SCXRD gas loading experiments. All authors contributed to the review of the final manuscript.

Conflicts of interest

There are no conflicts to declare.
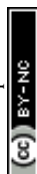
Acknowledgements

References

1 S. Kitagawa, *Angew. Chem., Int. Ed.*, 2015, **54**, 10686–10687.
2 M. M. Deegan, M. R. Dworzak, A. J. Gosselin, K. J. Korman and E. D. Bloch, *Chem.–Eur. J.*, 2021, **27**, 4531–4547.
3 H. Patel, S. H. Je, J. Park, D. P. Chen, Y. Jung, C. T. Yavuz and A. Coskun, *Nat. Commun.*, 2013, **4**, 1357–1364.
4 V. Rozyyev, D. Thirion, R. Ullah, J. Lee, M. Jung, H. Oh and M. Atilan, *Nat. Energy*, 2019, **4**, 604–611.
5 Z. Wu, V. Wee, X. Ma and D. Zhao, *Adv. Sustainable Syst.*, 2021, **5**, 2000200.
6 J. J. Perry, J. A. Perman and M. J. Zaworotko, *Chem. Soc. Rev.*, 2009, **38**, 1400–1417.
7 T. R. Cook, Y.-R. Zheng and P. J. Stang, *Chem. Rev.*, 2012, **113**, 734–777.
8 Z. Chen, M. C. Wasson, R. J. Drout, L. Robison, K. B. Idrees, J. G. Knapp, F. A. Son, X. Zhang, W. Hierse, C. Kuhn, S. Marx, B. Hernandez and O. K. Farha, *Faraday Discuss.*, 2021, **225**, 9–69.
9 P. Z. Moghadam, A. Li, S. b. Wiggin, A. Tao, A. G. P. Maloney, P. A. Wood, S. C. Ward and D. Fairen-Jimenez, *Chem. Mater.*, 2017, **29**(7), 2618–2625.
10 P. Z. Moghadam, A. Li, X.-W. Liu, R. Bueno-Perez, S.-D. Wang, S. B. Wiggin, P. A. Wood and D. Fairen-Jimenez, *Chem. Sci.*, 2020, **11**, 8373–8387.

16024 | *J. Mater. Chem. A*, 2023, **11**, 16019–16026

This journal is © The Royal Society of Chemistry 2023

11 H. Furukawa, K. E. Cordova, M. O'Keeffe and O. M. Yaghi, *Science*, 2013, **341**, 1230444.

12 D. Farrusseng, *Metal-Organic Frameworks: Applications from Catalysis to Gas Storage*, Wiley, 2011.

13 S. Kitagawa, R. Kitaura and S.-I. Noro, *Angew. Chem., Int. Ed.*, 2004, **43**, 2334–2375.

14 D. J. O'Hearn, A. Bajpai and M. J. Zaworotko, *Small*, 2021, 2006351.

15 S. R. Batten, S. M. Neville and D. R. Turner, *Coordination Polymers: Design, Analysis and Application*, The Royal Society of Chemistry, Cambridge, UK, 2009.

16 S.-Q. Wang, S. Mukherjee and M. J. Zaworotko, *Faraday Discuss.*, 2021, **231**, 9–50.

17 S. Krause, N. Hosono and S. Kitagawa, *Angew. Chem., Int. Ed.*, 2020, **59**, 15325–15341.

18 Z. Chen, P. Li, R. Anderson, X. Wang, X. Zhang, L. Robison, L. R. Redfern, S. Moribe, T. Islamoglu, D. A. Gómez-Gualdrón, T. Yildirim, J. F. Stoddart and O. M. Farha, *Science*, 2020, **368**, 297–303.

19 N. A. Ramsahye, T.-K. Trung, S. Bourrelly, Q.-Y. Yang, T. Devic, G. Maurin, P. Horcajada, P. L. Llewellyn, P. Yot, C. Serre, Y. Filinchuk, F. Fajula, G. Ferey and P. Trens, *J. Phys. Chem. C*, 2011, **115**, 18683–18695.

20 T. Devic, F. Salles, S. Bourrelly, B. Moulin, G. Maurin, P. Horcajada, C. Serre, A. Vimont, J.-C. Lavalley, H. Leclerc, G. Clet, M. Daturi, P. L. Llewellyn, Y. Filinchuk and G. Ferey, *J. Mater. Chem.*, 2012, **22**, 10266–10273.

21 M. K. Taylor, T. Runčevski, J. Oktawiec, M. I. Gonzalez, R. L. Siegelman, J. A. Mason, J. Ye, C. M. Brown and J. R. Long, *J. Am. Chem. Soc.*, 2016, **138**, 15019–15026.

22 A.-X. Zhu, Q.-Y. Yang, A. Kumar, C. Crowley, S. Mukherjee, K.-J. Chen, S.-Q. Wang, D. O'Nolan, M. Shivanna and M. J. Zaworotko, *J. Am. Chem. Soc.*, 2018, **140**, 15572–15576.

23 A.-X. Zhu, Q.-Y. Yang, S. Mukherjee, A. Kumar, C.-H. Deng, A. A. Bezrukov, M. Shivanna and M. J. Zaworotko, *Angew. Chem., Int. Ed.*, 2019, **58**, 18212–18217.

24 S. Bourrelly, P. L. Llewellyn, C. Serre, F. Millange, T. Loiseau and G. Férey, *J. Am. Chem. Soc.*, 2005, **127**, 13519–13521.

25 P. L. Llewellyn, P. Horcajada, G. Maurin, T. Devic, N. Rosenbach, S. Bourrelly, C. Serre, D. Vincent, S. LoeraSerna, Y. Filinchuk and G. Ferey, *J. Am. Chem. Soc.*, 2009, **131**, 13002–13008.

26 J. P. Mowat, V. R. Seymour, J. M. Griffin, S. P. Thompson, A. M. Slawin, D. Fairen-Jimenez, T. Düren, S. E. Ashbrook and P. A. Wright, *Dalton Trans.*, 2012, **41**, 3937–3941.

27 S. Galli, N. Masciocchi, V. Colombo, A. Maspero, G. Palmisano, F. J. López-Garzón, M. Domingo-Garcia, I. Fernández-Morales, E. Barea and J. A. R. Navarro, *Chem. Mater.*, 2010, **22**, 1664–1672.

28 N. Klein, H. C. Hoffmann, A. Cadiau, J. Getzschmann, M. R. Lohe, S. Paasch, T. Heydenreich, K. Adil, I. Senkovska, E. Brunner and K. Stefan, *J. Mater. Chem.*, 2012, **22**, 10303–10312.

29 C. M. McGuirk, T. Runčevski, J. Oktawiec, A. Turkiewicz, M. K. Taylor and J. R. Long, *J. Am. Chem. Soc.*, 2018, **140**, 15924–15933.

30 S.-Q. Wang, S. Darwish, D. Sensharma and M. J. Zaworotko, *Mater. Adv.*, 2022, **3**, 1240–1247.

31 S.-M. Wang, M. Shivanna, P. Lama, Q.-Y. Yang, L. J. Barbour and M. J. Zaworotko, *ChemSusChem*, 2023, e202300069.

32 K. Koupepidou, V. I. Nikolayenko, D. Sensharma, A. A. Bezrukov, M. Vandichel, S. Javan Nikkhah, D. C. Castell, K. A. Oyekan, N. Kumar, A. Subanbekova, W. G. Vandenberghe, K. Tan, L. J. Barbour and M. J. Zaworotko, *J. Am. Chem. Soc.*, 2023, **145**(18), 10197–10207.

33 J. L. Atwood, L. J. Barbour, A. Jerga and B. L. Schottel, *Science*, 2002, **298**, 1000–1002.

34 L. J. Barbour, *Chem. Commun.*, 2006, 1163–1168.

35 J. L. Atwood, L. J. Barbour and A. Jerga, *Angew. Chem., Int. Ed.*, 2004, **43**, 2948–2950.

36 J. A. Riddle, J. C. Bollinger and D. Lee, *Angew. Chem., Int. Ed.*, 2005, **44**, 6689–6693.

37 P. K. Thallapally, T. B. Wirsig, L. J. Barbour and J. L. Atwood, *Chem. Commun.*, 2005, 4420–4422.

38 P. K. Thallapally, B. P. Mcgrail, S. J. Dalgarno, H. T. Schaef, J. Tian and J. L. Atwood, *Nat. Mater.*, 2008, 7, 146–150.

39 J. T. Jones, A. D. Holden, T. Mitra, T. Hasell, D. J. Adams, K. E. Jelfs, A. Trewin, D. J. Willock, G. M. Day, J. Bacsa, A. Steiner and A. I. Cooper, *Angew. Chem., Int. Ed.*, 2011, **50**, 749–753.

40 D. Holden, S. Y. Chong, L. Chen, K. E. Jelfs, T. Hasella and A. I. Cooper, *Chem. Sci.*, 2016, 7, 4875–4879.

41 I. Brekalo, D. E. Deliz, L. J. Barbour, M. D. Ward, T. Friscic and T. Holman, *Angew. Chem., Int. Ed.*, 2020, **59**, 1997–2002.

42 D. Tanaka, K. Nakagawa, M. Higuchi, S. Horike, Y. Kubota, T. C. Kobayashi, M. Takata and S. Kitagawa, *Angew. Chem., Int. Ed.*, 2008, **47**, 3914–3918.

43 H. Sato, W. Kosaka, R. Matsuda, A. Hori, Y. Hijikata, R. V. Belosludov, S. Sakaki, M. Takata and S. Kitagawa, *Science*, 2014, **343**, 167–170.

44 C. Gu, N. Hosono, J.-J. Zheng, Y. Sato, S. Kusaka, S. Sakaki and S. Kitagawa, *Science*, 2019, **363**, 387–391.

45 D. P. van Heerden, V. J. Smith, H. Aggarwal and L. J. Barbour, *Angew. Chem., Int. Ed.*, 2021, **60**, 13430–13435.

46 V. I. Nikolayenko, D. C. Castell, D. Sensharma, M. Shivanna, L. Loots, K. A. Forrest, C. J. Solanilla, K.-I. Otake, S. Kitagawa, L. J. Barbour, B. Space and M. J. Zaworotko, *Nat. Chem.*, 2023, **15**, 542–549.

47 J. Seo, C. Bonneau, R. Matsuda, M. Takata and S. Kitagawa, *J. Am. Chem. Soc.*, 2011, **133**, 9005–9013.

48 S. Sen, N. Hosono, J.-J. Zheng, S. Kusaka, R. Matsuda, S. Sakaki and S. Kitagawa, *J. Am. Chem. Soc.*, 2017, **139**, 18313–18321.

49 L. J. Barbour, D. Das, T. Jacobs, G. O. Lloyd and V. J. Smith, *Supramolecular Chemistry: From Molecules to Nanomaterials*, John Wiley & Sons, Ltd, 2012.

50 M. L. Connolly, *Science*, 1983, **221**, 709–713.

51 M. L. Connolly, *J. Mol. Graphics*, 1993, **11**, 139–141.

52 S. Zuluaga, E. M. A. Fuentes-Fernandez, K. Tan, F. Xu, J. Li, Y. J. Chabal and T. Thonhauser, *J. Mater. Chem. A*, 2016, 4, 5176–5183.

This journal is © The Royal Society of Chemistry 2023

J. Mater. Chem. A, 2023, **11**, 16019–16026 | **16025**

53 Ü. Kökçam-Demir, A. Goldman, L. Esrafili, M. Gharib, A. Morsali, O. Weingart and C. Janiak, *Chem. Soc. Rev.*, 2020, **49**, 2751–2798.

54 B. P. Biswal, T. Panda and R. Banerjee, *Chem. Commun.*, 2012, **48**, 11868–11870.

55 A. Mallick, B. Garai, D. Díaz Díaz and R. Banerjee, *Angew. Chem., Int. Ed.*, 2013, **52**, 13755–13759.

56 A. L. Spek, *Acta Crystallogr., Sect. D: Biol. Crystallogr.*, 2008, **65**, 148–155.

57 A. L. Spek, *Acta Crystallogr., Sect. C: Struct. Chem.*, 2015, **71**, 9–18.

58 **https://arpa-e.energy.gov/?q=programs/move** for information on the methane storage targets set by DOE.

59 K. A. Forrest, G. Verma, Y. Ye, J. Ren, S. Ma, T. Pham and B. Space, *Chem. Phys. Rev.*, 2022, **3**, 021308.

60 C. M. Simon, J. Kim, D. A. Gomez-Gualdron, J. S. Camp, Y. G. Chung, R. L. Martin, R. Mercado, M. W. Deem, D. Gunter, M. Haranczyk, D. S. Sholl, R. l Q. Snurr and B. Smit, *Energy Environ. Sci.*, 2015, **8**, 1190–1199.

16026 | *J. Mater. Chem. A*, 2023, **11**, 16019–16026

This journal is © The Royal Society of Chemistry 2023